Nonlinear Dyn (2024) 112:22245–22256
https://doi.org/10.1007/s11071-024-10180-2

RESEARCH

Dynamical analysis of solitons, breathers and periodic rogue waves for the variable-coefficient fourth-order nonlinear Schrödinger equation

Ni Song · Yating Liu · Zhuyan Wen · Wenxiu Ma

Received: 14 July 2024 / Accepted: 14 August 2024 / Published online: 26 August 2024

Abstract This work focuses on higher-order localized waves for coupled variable-coefficient fourth-order nonlinear Schrödinger equation that describe the simultaneous propagation of optical pulses in an inhomogeneous optical fiber. Based on the Lax pair, N-th Darboux transformation is constructed and iterative expression of localized wave solutions are obtained. Three-dimensional animations are used to reveal the dynamical characteristics and evolution of nonautonomous localized waves solutions. Profiles and contour plots distributions of nonautonomous solitons, breathers, and rogue waves are shown. The variable coefficients functions $\gamma_1(t)$ and $\sigma(t)$ are discussed to reveal how the magnitude, shape, and position of background waves are affected. It is hopeful that results may provide theoretical basis for the research on the localized waves in an inhomogeneous optical fiber in the future.

Keywords Variable-coefficient equation · Generalized Darboux transformation · Localized wave solution

N. Song (✉) · Y. Liu · Z. Wen
Department of Mathematics, North University of China, Taiyuan 030051, Shanxi, China
e-mail: songni@nuc.edu.cn

W. Ma
Department of Mathematics, Zhejiang Normal University, Jinhua 321004, Zhejiang, China

Department of Mathematics, King Abdulaziz University, Jeddah 21589, Saudi Arabia

Department of Mathematics and Statistics, University of South Florida, Tampa, FL 33620-5700, USA

W. Ma (✉)
School of Mathematical and Statistical Sciences, North-West University, Mafikeng Campus, Private Bag X2046, Mmabatho 2735, South Africa
e-mail: mawx@cas.usf.edu

1 Introduction

The study of localized waves governed by nonlinear equations is a fascinating area of research that has attracted significant attention from researchers due to its wide range of applications in physics, mathematics, and engineering [1–3]. Localized waves can be categorized as solitons, breathers, and rogue waves [4]. Solitons are stable wave packets that maintain their shape and amplitude over long distance. They are characterized by the particle-like properties, which mean solitons can interact with each other without losing their own form [5,6]. Breathers are special type of nonlinear waves that exhibit a breathing or pulsating behavior [7]. Unlike solitons, breathers involve a periodic exchange of energy with the surrounding medium, which can be thought as localized oscillations. Breathers are important in understanding certain phenomena such as those occurring in optical fibers and mechanical systems [8]. Rogue waves are transient and highly energetic waves that occur unexpectedly and have a much larger amplitude than the surrounding waves. Rogue waves are

characterized by their sudden appearance, which have a significant impact on maritime activities and coastal structures. The amplitude of the rogue wave is typically at least twice that of waves in the background field, making them a significant concern for safety and stability [9–11].

Each type of localized waves has unique characteristics and behaviors. Their study contributes to a broader understanding of wave phenomena in nonlinear systems. In the nonlinear science, many nonlinear evolution equations are derived from the integrable systems, so that many phenomena can be described by the integrable equations. In recent decades, integrability theory has made great progress and has been widely used in many fields, such as optical fiber systems, plasma astrophysics, Bose–Einstein condensation, molecular dynamics, biology, and oceanography [12–17]. The currently available methods to find the N-th soliton solutions of an integral equation include the Riemann–Hilbert method [18], the Darboux-dressing method [19], and the Hirota bilinear method [20]. So far, the binary Darboux transformation method has been put forward for finding the soliton solutions of the focusing nonlocal nonlinear Schrödinger equation [21]. Also, periodic localized wave solutions have been successfully constructed by using the Bell polynomials approach, the PINN deep learning method, and the Darboux transformation [22–24]. The coupled variable-coefficient equation containing dispersion, self-steepening, and decay nonlinear response is more abundant than the one with constant-coefficient describing the nonlinear wave behavior [25–27]. On this basis, the variable-coefficient fourth-order nonlinear Schrödinger equation (NLS) is studied, which can be used to describe nonlinear transmission and interaction of ultrashort pulses in high-speed optical fiber communication systems, and nonlinear spin excitations in one-dimensional Heisenberg ferromagnetic chains [28–30],

$$
\begin{aligned}
&iq_{j,t}+\sigma(t)q_{j,xx}+\mu(t)q_j\sum_{l=1}^{3}|q_l|^2\\
&+\gamma_1(t)q_{j,xxxx}+\gamma_2(t)q_j\sum_{l=1}^{3}|q_l|^2\\
&+\gamma_3(t)q_{j,x}\sum_{l=1}^{3}q_lq_{l,x}^*+\gamma_4(t)q_{j,x}\sum_{l=1}^{3}q_lq_{l,x}^*\\
&+\gamma_5(t)q_{j,xx}\sum_{l=1}^{3}|q_l|^2\\
&+\gamma_6(t)q_j\sum_{l=1}^{3}q_l^*q_{l,xx}+\gamma_7(t)q_j\sum_{l=1}^{3}q_l^*q_{l,xx}\\
&+\gamma_8(t)q_j(\sum_{l=1}^{3}|q_l|^2)^2=0,\ (j=1,2,3),
\end{aligned}
\tag{1}
$$

where $q_j(x,t)$, $(j=1,2,3)$ are the amplitudes of molecular excitation, the subscripts x denotes partial derivatives with respect to the normalized propagation distance, t represents the retarded time, and the symbol $*$ indicates the complex conjugate. $\sigma(t)$ is the group velocity dispersion (GVD) coefficient, $\mu(t)$ is related to the self-phase modulation (SPM) coefficient, $\gamma_1(t)$ is the fourth-order dispersion coefficient, $\gamma_\alpha(t)(\alpha=2,...7)$ are the cubic nonlinear coefficients, and $\gamma_8(t)$ is the quintic nonlinear coefficient. Eq. (1) is completely integrable under the conditions,

$$
\begin{aligned}
&\mu(t)=2\sigma(t),\gamma_2(t)=2\gamma_1(t),\\
&\gamma_3(t)=2\gamma_1(t),\gamma_4(t)=6\gamma_1(t),\\
&\gamma_5(t)=4\gamma_1(t),\gamma_6(t)=4\gamma_1(t),\\
&\gamma_7(t)=2\gamma_1(t),\gamma_8(t)=6\gamma_1(t).
\end{aligned}
$$

Some studies have been conducted on two-component fourth-order nonlinear Schrödinger equations. For instance, Xu et al. [31] derived the soliton solutions using the Riemann-Hilbert method. Borluk et al. [32] investigated the orbital stability of solitary waves for the fourth-order nonlinear Schrödinger equation. Zhou et al. [33] obtained the vector breather waves and higher-order rogue waves for the coupled higher-order nonlinear Schrödinger equations. However, there are no reports on the solitons, breathers, and periodic rogue waves mixed interaction solutions for Eq. (1) by far. The aim of this paper is to construct N-order solutions of the localized waves for Eq. (1) using the generalized Darboux transformation. Specially, it is found that periodic rogue waves occur in the periodic background.

This paper will be prepared as follows. In Sect. 2, the generalized Darboux transformation is constructed, and the N-order localized wave solutions are derived. In Sect. 3, the fission and annihilation phenomena of solitons, breathers, and rogue waves for Eq. (1) are presented by three-dimensional animations. The inhomogeneity of the fiber affects the transmission of the localized waves, such as the width, amplitude, and derection

of propagation. It can be seen that solitons, breathers, and rogue waves are managed by appropriately selecting the controllable parameters.

2 Generalized Darboux transformation

In this section, we derive the solutions for Eq. (1). A Lax pair equation and a 4×4 eigenvalue problem and is considerd,

$$\begin{aligned} \Phi_x &= U\Phi, \\ \Phi_t &= V\Phi, \end{aligned} \tag{2}$$

with

$$U = \begin{pmatrix} -i\lambda & q_1 & q_2 & q_3 \\ -q_1^* & i\lambda & 0 & 0 \\ -q_2^* & 0 & i\lambda & 0 \\ -q_3^* & 0 & 0 & i\lambda \end{pmatrix}, V = \begin{pmatrix} V_{11} & V_{12} & V_{13} & V_{14} \\ V_{21} & V_{22} & V_{23} & V_{24} \\ V_{31} & V_{32} & V_{33} & V_{34} \\ V_{41} & V_{42} & V_{43} & V_{44} \end{pmatrix},$$

where $\Phi = (\phi, \varphi, \chi, \psi)^T$ is the vector solution of Eq. (2) and the superscript T represents the vector transpose, $q_j (j = 1, 2, 3)$ are potential functions, λ is the spectral parameter and $\phi, \varphi, \chi, \psi$ are the complex functions related to x, t and λ.

$$\begin{aligned} V_{11} = {} & 8i\gamma_1(t)\lambda^4 - 2i\left[\sigma(t) + 2\gamma_1(t)\sum_{l=1}^{3}|q_l|^2\right]\lambda^2 \\ & +2\gamma_1(t)\sum_{l=1}^{3}\left(q_l^* q_{l,x} - q_l q_{l,x}^*\right)\lambda \\ & -i\gamma_1(t)\sum_{l=1}^{3}|q_{l,x}|^2 - \sum_{l=1}^{3}\left(q_l^* q_{l,xx} + q_l q_{l,xx}^*\right) \\ & -3\left(\sum_{l=1}^{3}|q_l|^2\right)^2\Bigg] + i\sigma(t)\sum_{l=1}^{3}|q_l|^2, \\ V_{1,s} = {} & -8\gamma_1(t)q_{s-1}\lambda^3 - 4iq_{s-1,x}\lambda^2 \\ & +2\Big[\sigma(t)q_{s-1} + \gamma_1(t)q_{s-1,xx} + 2\gamma_1(t)q_{s-1} \\ & \sum_{l=1}^{3}|q_l|^2\Big]\lambda + i\gamma_1(t)\Big[q_{s-1,xxx} \\ & +3q_{s-1,x}\sum_{l=1}^{3}|q_l|^2 \\ & +3q_{s-1,x}\sum_{l=1}^{2}q_l^* q_{l,x}\Big] + i\sigma(t)q_{s-1,x}, \\ V_{s,1} = {} & V_{1,s}^*, \end{aligned}$$

$$\begin{aligned} V_{ss} = {} & 8i\gamma_1(t)\lambda^4 - 2i\left[\sigma(t) + 2\gamma_1(t)\sum_{l=1}^{3}|q_{s-1}|^2\right]\lambda^2 \\ & +2\gamma_1(t)\sum_{l=1}^{3}\left(q_{s-1}^* q_{s-1,x} - q_{s-1}q_{s-1,x}^*\right)\lambda \\ & -3i\gamma_1(t)|q_{s-1}|^2\sum_{l=1}^{3}|q_l|^2 + i\gamma_1(t)\Big[|q_{s-1,x}|^2 \\ & -q_{s-1}q_{s-1,xx}^* - q_{s-1}^* q_{s-1,xx}\Big] \\ & -i\sigma(t)|q_{s-1}|^2, (s = 2, 3, 4) \end{aligned}$$

It can be easily proved that U and V satisfy the compatibility condition $U_t - V_x + UV - VU = 0$.

The Darboux matrix T can be constructed as follows,

$$T = \lambda I - H\Lambda H^{-1}, \tag{3}$$

where

$$H = \begin{pmatrix} \phi_1 & \varphi_1^* & \chi_1^* & \psi_1^* \\ \varphi_1 & -\phi_1^* & 0 & 0 \\ \chi_1 & 0 & -\phi_1^* & 0 \\ \psi_1 & 0 & 0 & -\phi_1^* \end{pmatrix}, \Lambda = \begin{pmatrix} \lambda_1 & 0 & 0 & 0 \\ 0 & \lambda_1^* & 0 & 0 \\ 0 & 0 & \lambda_1^* & 0 \\ 0 & 0 & 0 & \lambda_1^* \end{pmatrix}.$$

I is the identity matrix, $\Phi_1 = (\phi_1, \varphi_1, \chi_1, \psi_1)^T = \Phi_1(\lambda_1, \eta)$ refers to the eigenfunction of Eq. (2) corresponding to the spectral parameters $\lambda = \lambda_1$ and seed solutions $q_1 = q_1[0], q_2 = q_2[0]$ and $q_3 = q_3[0]$. Thus, the classical Darboux transformatin is defined,

$$\begin{aligned} & \lambda = \lambda_k, \Phi_k = (\phi_k, \varphi_k, \chi_k, \psi_k)^T, (k = 1, 2, \ldots N) \\ & \Phi_N[N-1] = T[N-1]\,T[N-2]\cdots T[1]\,\Phi_N \end{aligned}$$

$$q_1[1] = q_1[0] - 2i(\lambda_1 - \lambda_1^*)\frac{\phi_k^*[k-1]\varphi_k[k-1]}{|\phi_k[k-1]|^2 + |\varphi_k[k-1]|^2 + |\chi_k[k-1]|^2 + |\psi_k[k-1]|^2}, \tag{4}$$

$$q_2[1] = q_2[0] - 2i(\lambda_1 - \lambda_1^*)\frac{\phi_k^*[k-1]\chi_k[k-1]}{|\phi_k[k-1]|^2 + |\varphi_k[k-1]|^2 + |\chi_k[k-1]|^2 + |\psi_k[k-1]|^2}, \tag{5}$$

$$q_3[1] = q_3[0] - 2i(\lambda_1 - \lambda_1^*)\frac{\phi_k^*[k-1]\psi_k[k-1]}{|\phi_k[k-1]|^2 + |\varphi_k[k-1]|^2 + |\chi_k[k-1]|^2 + |\psi_k[k-1]|^2}. \tag{6}$$

where

$$T[k] = \lambda_k + 1I - H[k-1]\Lambda_k H_1[k-1]^{-1},$$

$$\Phi_1[k-1] = (T[k-1]T[k-2]\cdots T[1])\lambda = \lambda_k \Phi_k,$$

$$H_1[k-1] = \begin{pmatrix} \phi_1[k-1] & \varphi_1^*[k-1] & \chi_1^*[k-1] & \psi_1^*[k-1] \\ \varphi_1[k-1] & -\phi_1^*[k-1] & 0 & 0 \\ \chi_1[k-1] & 0 & -\phi_1^*[k-1] & 0 \\ \psi_1[k-1] & 0 & 0 & -\phi_1^*[k-1] \end{pmatrix},$$

$$\Lambda_k = \begin{pmatrix} \lambda_k & 0 & 0 & 0 \\ 0 & \lambda_k^* & 0 & 0 \\ 0 & 0 & \lambda_k^* & 0 \\ 0 & 0 & 0 & \lambda_k^* \end{pmatrix}.$$

Based on the above classical Darboux transformation, the generalized Darboux transformation of Eq. (1) is constructed. Assuming that $\Phi_1 = (\phi_1, \varphi_1, \chi_1, \psi_1)^T = \Phi_1(\lambda_1, \eta)$ is a solution of Eq. (2) and η is a small parameter, then Φ_1 is expanded as the Taylor series at $\eta = 0$,

$$\Phi_1 = \Phi_1[0] + \Phi_1[1]\eta + \Phi_1[2]\eta^2 + \cdots + \Phi_1[N]\eta^N + \cdots$$

where

$$\Phi_1^{[k]} = \frac{1}{k!}\frac{\partial^k}{\partial \lambda^k}$$
$$\Phi_1(\lambda)|_{\lambda=\lambda_1} = (\phi_1^{[k]}, \varphi_1^{[k]}, \chi_1^{[k]}, \psi_1^{[k]})^T, \quad (k = 0, 1, 2, \cdots, N)$$

It can be easily confirmed that $\Phi_1^{[0]} = \Phi_1[0]$ is a solution of Eq. (1) with $\lambda = \lambda_1$, $q_1 = q_1[0], q_2 = q_2[0]$ and $q_3 = q_3[0]$. Thus, the generalized Darboux transformation of (N-1)-th can be defined as follows,

$$\Phi_1[N-1] = \Phi_1^{[0]} + \left[\sum_{l=1}^{N-1} T_1[l]\right]\Phi_1^{[1]} + \left[\sum_{l=1}^{N-1}\sum_{k>l}^{N-1} T_1[k]T_1[l]\right]\Phi_1^{[2]} + \cdots + [T_1[N-1]T_1[N-2]\cdots T_1[1]]\,\Phi_1^{[N-1]}, \tag{7}$$

$$q_1[N] = q_1[N-1] - 2i(\lambda_1 - \lambda_1^*)\frac{\phi_k^*[k-1]\varphi_k[k-1]}{|\phi_k[k-1]|^2 + |\varphi_k[k-1]|^2 + |\chi_k[k-1]|^2 + |\psi_k[k-1]|^2}, \tag{8}$$

$$q_2[N] = q_2[N-1] - 2i(\lambda_1 - \lambda_1^*)\frac{\phi_k^*[k-1]\chi_k[k-1]}{|\phi_k[k-1]|^2 + |\varphi_k[k-1]|^2 + |\chi_k[k-1]|^2 + |\psi_k[k-1]|^2}, \tag{9}$$

$$q_3[N] = q_3[N-1] - 2i(\lambda_1 - \lambda_1^*)\frac{\phi_k^*[k-1]\psi_k[k-1]}{|\phi_k[k-1]|^2 + |\varphi_k[k-1]|^2 + |\chi_k[k-1]|^2 + |\psi_k[k-1]|^2}. \tag{10}$$

where

$$T_1[k] = \lambda_1 I - H_1[k-1]\Lambda_1 H_1[k-1]^{-1},$$
$$\Phi_1[N-1] = (\phi_1[N-1], \varphi_1[N-1], \chi_1[N-1], \psi_1[N-1])^T,$$

$$H_1[k-1] = \begin{pmatrix} \phi_1[k-1] & \varphi_1^*[k-1] & \chi_1^*[k-1] & \psi_1^*[k-1] \\ \varphi_1[k-1] & -\phi_1^*[k-1] & 0 & 0 \\ \chi_1[k-1] & 0 & -\phi_1^*[k-1] & 0 \\ \psi_1[k-1] & 0 & 0 & -\phi_1^*[k-1] \end{pmatrix},$$

$$\Lambda_1 = \begin{pmatrix} \lambda_1 & 0 & 0 & 0 \\ 0 & \lambda_1^* & 0 & 0 \\ 0 & 0 & \lambda_1^* & 0 \\ 0 & 0 & 0 & \lambda_1^* \end{pmatrix}.$$

3 Dynamics of the localized waves

Supposing that the seed solutions of Eq. (1) are $q_1^{[0]} = a_1 e^{i\omega}$, $q_2^{[0]} = a_2 e^{i\omega}$ and $q_3^{[0]} = a_3 e^{i\omega}$, where $\omega(t) = \int 2\sigma(t)(a_1^2 + a_2^2 + a_3^2) + 6\gamma_1(t)(a_1^2 + a_2^2 + a_3^2)^2 dt$, and a_1, a_2, a_3 are arbitrary real constants. The corresponding basic vector solution at $\lambda = \left(i\sqrt{a_1^2 + a_2^2 + a_3^2}\right)(1 + \eta^2)$ can be written as follows,

$$\underset{\Phi_1(\eta)}{} = \begin{pmatrix} \left(C_1 e^{M_1+M_2} - C_2 e^{M_1-M_2}\right) e^{\frac{i}{2}\omega} \\ \rho_1\left(C_1 e^{M_1-M_2} - C_2 e^{M_1+M_2}\right) e^{-\frac{i}{2}\omega} + \alpha a_3 e^{M_3} \\ \rho_2\left(C_1 e^{M_1-M_2} - C_2 e^{M_1+M_2}\right) e^{-\frac{i}{2}\omega} + \beta a_3 e^{M_3} \\ \rho_3\left(C_1 e^{M_1-M_2} - C_2 e^{M_1+M_2}\right) e^{-\frac{i}{2}\omega} - (\alpha a_1 + \beta a_2) e^{M_3} \end{pmatrix}, \tag{11}$$

with

$$\rho_1 = \frac{a_1}{\sqrt{a_1^2 + a_2^2 + a_3^2}}, \rho_2 = \frac{a_2}{\sqrt{a_1^2 + a_2^2 + a_3^2}},$$
$$\rho_3 = \frac{a_3}{\sqrt{a_1^2 + a_2^2 + a_3^2}},$$
$$C_1 = \frac{\sqrt{\lambda - \sqrt{\lambda^2 + a_1^2 + a_2^2 + a_3^2}}}{\sqrt{\lambda^2 + a_1^2 + a_2^2 + a_3^2}},$$
$$C_2 = \frac{\sqrt{\lambda + \sqrt{\lambda^2 + a_1^2 + a_2^2 + a_3^2}}}{\sqrt{\lambda^2 + a_1^2 + a_2^2 + a_3^2}},$$
$$M_1 = 0,$$

$$M_2 = i\sqrt{\lambda^2+a_1^2+a_2^2+a_3^2}(x-4\gamma_1(t)\lambda^3 t+\lambda t(\sigma(t)$$
$$+2\gamma_1(t)(a_1^2+a_2^2+a_3^2))t+\Omega(\eta)),$$
$$M_3 = i\lambda x+(-8i\gamma_1(t)\lambda^4+2i\sigma(t)\lambda^2)t,$$
$$\Omega(\eta)=\sum_{k=1}^{N} s_k\eta^{2k},\ s_k=m_k+in_k,\ (k=1,2,\cdots N),$$

where α, β, m_k and n_k are arbitrary real constants and $\Omega(\eta)$ is a separation function. The vector function $\Phi_1(\eta)$ at $\eta = 0$ can be expanded by using the Taylor series as follows,

$$\Phi_1(\eta)=\Phi_1^{[0]}+\Phi_1^{[1]}\eta^2+\Phi_1^{[2]}\eta^4+\Phi_1^{[3]}\eta^6+\cdots, \tag{12}$$

where

$$\Phi_1(\eta) = (\phi_1^{[k]},\varphi_1^{[k]},\chi_1^{[k]},\psi_1^{[k]})^T$$
$$= \frac{1}{(2k)!}\frac{\partial^{2k}\Phi_1}{\partial\eta^{2k}}|_{\eta=0},(k=0,1,2,\cdots).$$

The expression $\Phi_1^{[k]} = \left(\phi_1^{[k]},\varphi_1^{[k]},\chi_1^{[k]},\psi_1^{[k]}\right)^T (k = 0, 1, 2\cdots)$ are complex, which form are omitted here. Furthermore, the first- and second-order localized wave solutions of Eq. (1) are considered, and the dynamical characteristics of localized waves are analyzed using evolutionary plots.

Obviously, when $q_1 = q_1[0], q_2 = q_2[0], q_3 = q_3[0]$, λ=λ_1 and $\Phi_1^{[0]} = \left(\phi_1^{[0]},\varphi_1^{[0]},\chi_1^{[0]},\psi_1^{[0]}\right)^T$ are seed solutions of the Lax pair,. According to Eqs. (8–10), the first-order localized wave solutions of Eq. (1) can be obtained as follows,

$$q_1[1] = q_1[0]-2i(\lambda_1-\lambda_1^*)\frac{\phi_1^*[0]\varphi_1[0]}{|\phi_1[0]|^2+|\varphi_1[0]|^2+|\chi_1[0]|^2+|\psi_1[0]|^2}, \tag{13}$$

$$q_2[1] = q_2[0]-2i(\lambda_1-\lambda_1^*)\frac{\phi_1^*[0]\chi_1[0]}{|\phi_1[0]|^2+|\varphi_1[0]|^2+|\chi_1[0]|^2+|\psi_1[0]|^2}, \tag{14}$$

$$q_3[1] = q_3[0]-2i(\lambda_1-\lambda_1^*)\frac{\phi_1^*[0]\psi_1[0]}{|\phi_1[0]|^2+|\varphi_1[0]|^2+|\chi_1[0]|^2+|\psi_1[0]|^2}. \tag{15}$$

The evolutionary plots of the first-order localized waves are derived by altering values of seven free parameters: $\gamma_1(t), \sigma(t), a_1, a_2, a_3, \alpha$ and β. The dynamics of the first-order localized waves are analyzed.

(1) Figure 1 depicts the interaction between the first-order rogue waves and the bright-dark solitons. When the coefficients $\gamma_1(t)$ and $\sigma(t)$ are both selected as constants, the propagation direction of solitons are parallel to the t-axis, as exhibited in Fig. 1a, b, and c. When $\gamma_1(t) = \sigma(t) = 5t^4$, the solitons bend at $t = 0$ and are exhibited the shape of $''V''$, as displayed in Fig. 1d, e, and f. When the coefficients $\gamma_1(t)$ and $\sigma(t)$ are periodic functions, periodic propagation of the rogue waves and solitons occur as shown in Fig. 1g, h, and i. Figure 1j, k and l show the profile of Fig. 1a, b and c at $t = 0$, respectively. It can be seen that the amplitude of the rogue wave of the component $q_1[1]$ is higher than that of $q_2[1]$ for the value of parameter a_1 is bigger than the the parameter a_2, as shown in Fig. 1j and k. In addition, in the zero-amplitude background, only a bright soliton is found while the first-order rogue waves can not easily detected, as demonstrated in Fig. 1c, e, f, i and l.

(2) Figure 2 depicts the collision of the first-order rogue waves and breathers. When the coefficients $\gamma_1(t)$ and $\sigma(t)$ are constants, the interaction between the common first-order rogue waves and the bright-dark breathers are illustrated, as shown in Fig. 2a, b and c. When $\gamma_1(t)$ and $\sigma(t)$ are both exponential functions, the breathers take the shape of $''V''$, as shown in Fig. 2 d, e and f. When $\gamma_1(t)$ and $\sigma(t)$ are periodic functions, the periodic rogue waves coexist with the periodic breather, as demonstrated in Fig. 2g, h and i.

Based on the following limit formula

$$\Phi_1[1] = \lim_{\eta\to 0}\frac{T[1]|_{\lambda=\lambda_1(1+\eta^2)}\Phi_1}{\eta^2} = \lim_{\eta\to 0}\frac{(\lambda_1\eta^2+T_1[1])\Phi_1}{\eta^2} = \lambda_1\Phi_1^{[0]}+T_1[1]\Phi_1^{[1]}. \tag{16}$$

and Eqs. (8–10), with $T_1[1] = \lambda_1 I - H_1[0]\Lambda_1 H_1[0]^{-1}$ and $\Phi_1^{[1]} = (\phi_1^{[1]}\varphi_1^{[1]},\psi_1^{[1]},\chi_1^{[1]})^T$, the second-order localized wave solutions of Eq. (1) can be obtained,

$$q_1[2] = q_1[1]-2i(\lambda_1-\lambda_1^*)\frac{\phi_1^*[1]\varphi_1[1]}{|\phi_1[1]|^2+|\varphi_1[1]|^2+|\chi_1[1]|^2+|\psi_1[1]|^2}, \tag{17}$$

$$q_2[2] = q_2[1]-2i(\lambda_1-\lambda_1^*)\frac{\phi_1^*[1]\chi_1[1]}{|\phi_1[1]|^2+|\varphi_1[1]|^2+|\chi_1[1]|^2+|\psi_1[1]|^2}, \tag{18}$$

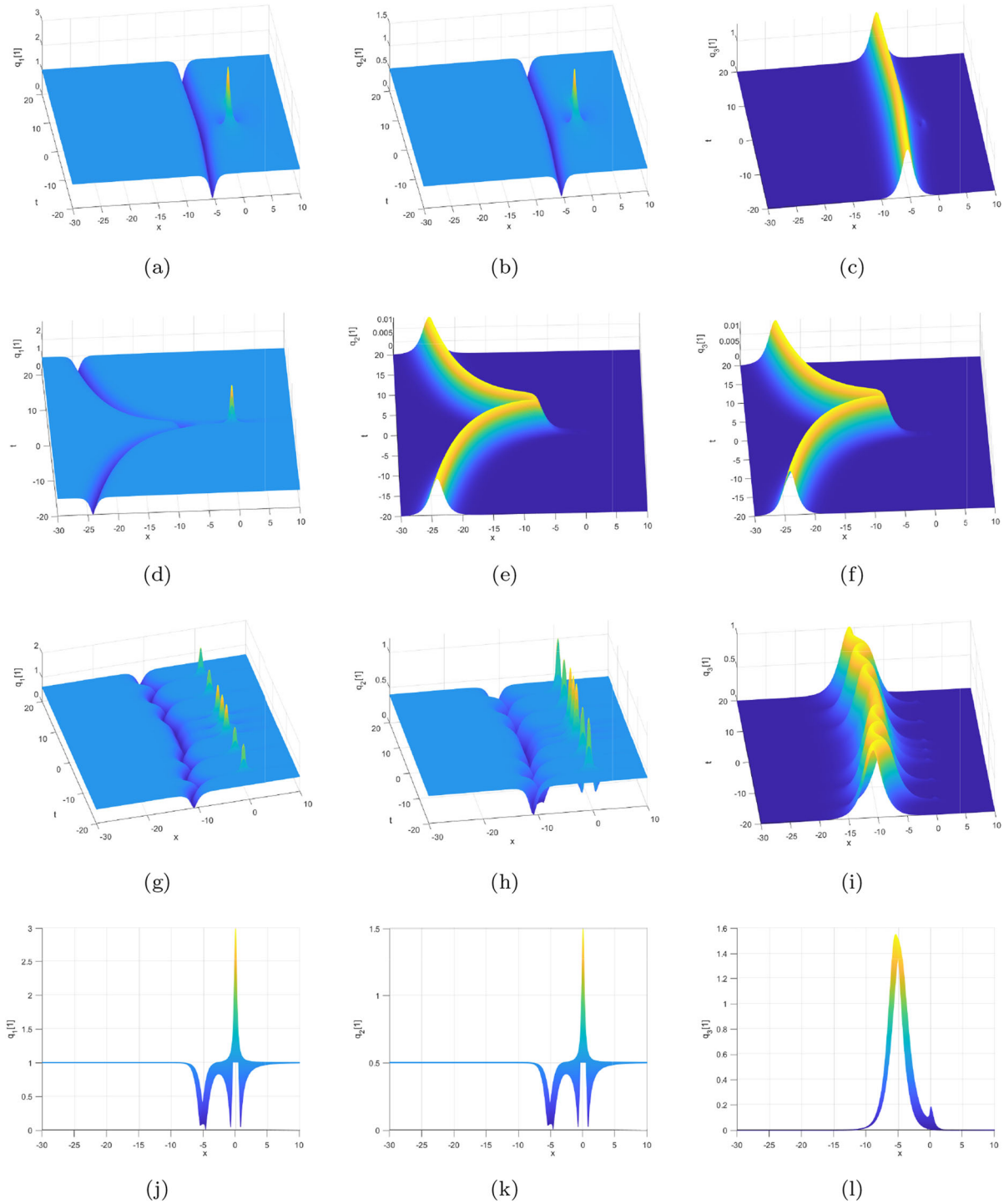

Fig. 1 Evolution diagrams of the first-order localized waves at **a–c** and **j–l** $\gamma_1(t) = 0.05, \sigma(t) = 0.05, a_1 = 1, a_2 = 0.5, a_3 = 0, \alpha = 0.05, \beta = 0.05$; **d–f** $\gamma_1(t) = 5t^4, \sigma(t) = 5t^4, a_1 = 1, a_2 = 0, a_3 = 0, \alpha = 0.01, \beta = 0.01$; **g–i** $\gamma_1(t) = \cos(\frac{t}{2}), \sigma(t) = \cos(\frac{t}{2}), a_1 = 0.6, a_2 = 0.4, a_3 = 0, \alpha = 0.05, \beta = 0.05$

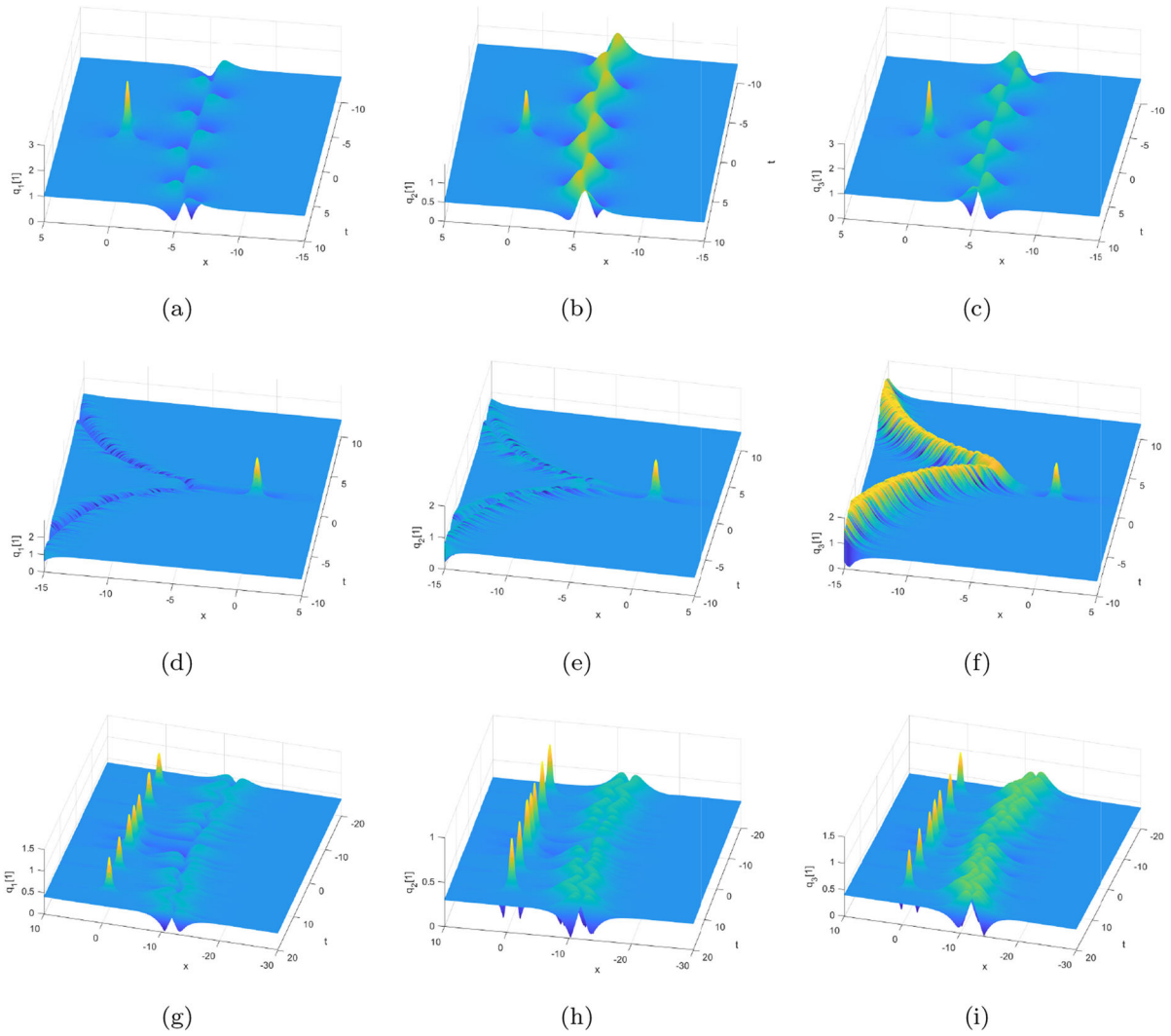

Fig. 2 Evolution diagrams of the first-order localized waves at **a–c** $\gamma(t) = 0.05, \sigma(t) = 0.05, a_1 = 1, a_2 = 0.5, a_3 = 1, \alpha = 0.005, \beta = 0.005$; **d–f** $\gamma(t) = 5t^4, \sigma(t) = 5t^4, a_1 = 1, a_2 = 0.6, a_3 = 0.6, \alpha = 0.01, \beta = 0.01$; **g–i** $\gamma(t) = \cos(\frac{t}{2}), \sigma(t) = \cos(\frac{t}{2}), a_1 = 0.4, a_2 = 0.3, a_3 = 0.4, \alpha = 0.05, \beta = 0.05$

$$q_3[2] = q_3[1] - 2i(\lambda_1 - \lambda_1^*) \frac{\phi_1^*[1]\psi_1[1]}{|\phi_1[1]|^2 + |\varphi_1[1]|^2 + |\chi_1[1]|^2 + |\psi_1[1]|^2}. \tag{19}$$

Furthermore, the dynamical characteristics of the second-order localized wave solutions are analyzed by choosing different values for nine parameters $\gamma_1(t), \sigma(t), a_1, a_2, a_3, \alpha, \beta, m_1$ and n_1, which are discussed in the following cases.

(3) Dynamics of the localized waves in the component $q_1[2]$ is studied in Figure 3, the other components are also studied in the same way. It is exhibited the impact on the localized waves with the changing of the parameters by using the contour plots. When $\gamma_1(t)$ and $\sigma(t)$ are constants, the interaction between the second-order rogue waves and the bright-dark solitons can be observed in Fig. 3a, b and c. If $m_1 = n_1 = 0$, the second-order rogue waves appear, as demonstrated in Fig. 3a. Changing the parameters $m_1 = n_1 = 1$, the second-order rogue waves are separated into three first-order rogue waves with a small triangular arrangement due to the separation function $\Omega(\eta)$, as dis-

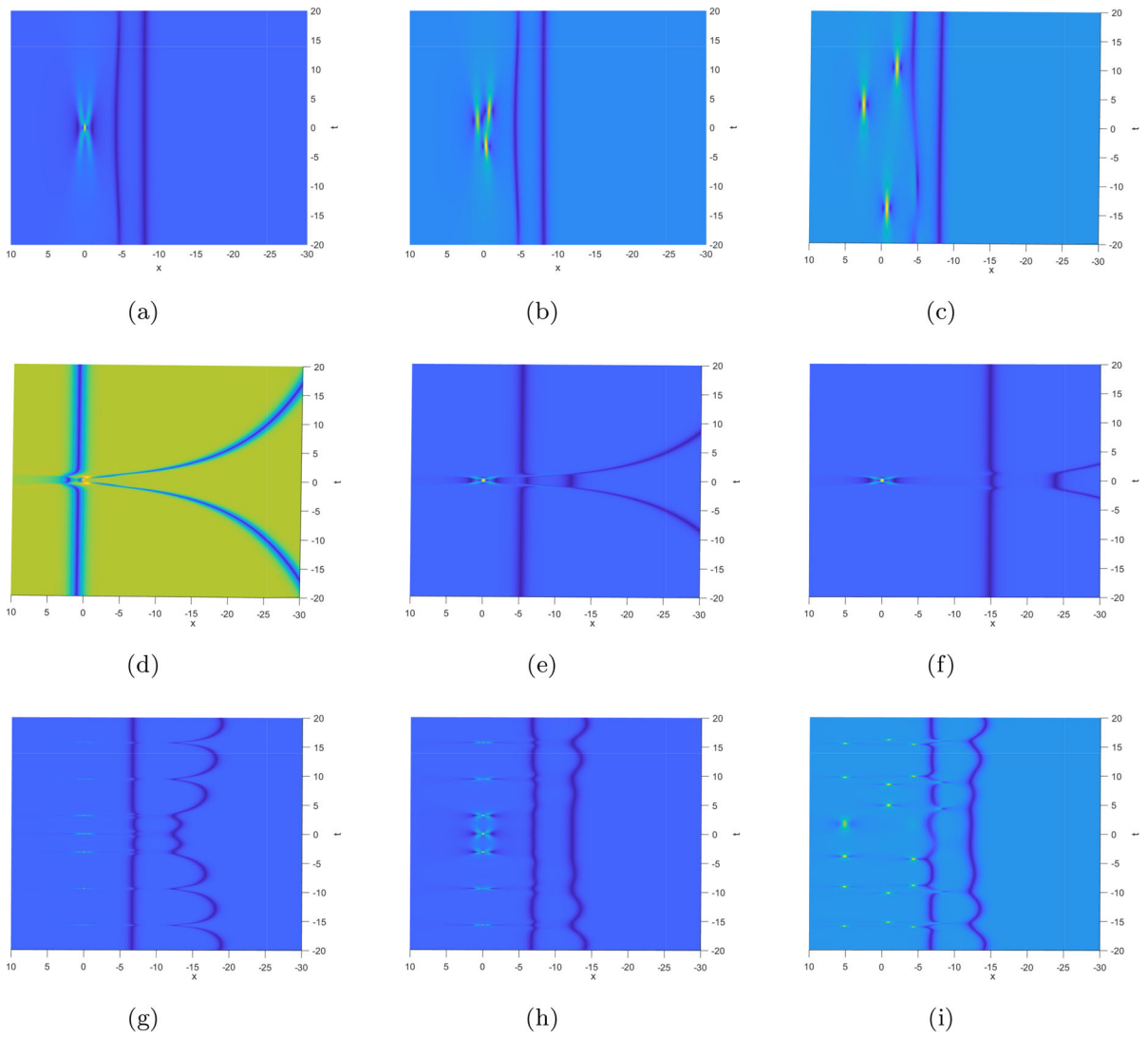

Fig. 3 Contour plots of the second-order localized waves at **a** $\gamma(t) = 0, \sigma(t) = 0.1, a_1 = 1.8, a_2 = 0, a_3 = 0, \alpha = 0.001, \beta = 0.001, m_1 = 0, n_1 = 0$; **b** $\gamma(t) = 0, \sigma(t) = 0.1, a_1 = 1.8, a_2 = 0, a_3 = 0, \alpha = 0.001, \beta = 0.001, m_1 = 1, n_1 = 1$; **c** $\gamma(t) = 0, \sigma(t) = 0.1, a_1 = 1.8, a_2 = 0, a_3 = 0, \alpha = 0.001, \beta = 0.001, m_1 = 20, n_1 = 20$; **d** $\gamma(t) = t^2, \sigma(t) = t^2, a_1 = 0, a_2 = 0, a_3 = 1, m_1 = 0, n_1 = 0, \alpha = 5, \beta = 5$; **e** $\gamma(t) = t^2, \sigma(t) = t^2, a_1 = 0, a_2 = 0, a_3 = 1, m_1 = 0, n_1 = 0, \alpha = 0.01, \beta = 0.01$; **f** $\gamma(t) = t^2, \sigma(t) = t^2, a_1 = 0, a_2 = 0, a_3 = 1, m_1 = 0, n_1 = 0, \alpha = 0.0001, \beta = 0.0001$; **g** $\gamma(t) = 0, \sigma(t) = 10\cos(\frac{t}{2}), a_1 = 1, a_2 = 0, a_3 = 0, \alpha = 0.001, \beta = 0.001, m_1 = 0, n_1 = 0$; **h** $\gamma(t) = 0, \sigma(t) = \cos(\frac{t}{2}), a_1 = 1, a_2 = 0, a_3 = 0, \alpha = 0.001, \beta = 0.001, m_1 = 0, n_1 = 0$; **i** $\gamma(t) = 0, \sigma(t) = \cos(\frac{t}{2}), a_1 = 1, a_2 = 0, a_3 = 0, \alpha = 0.001, \beta = 0.001, m_1 = 100, n_1 = 200$

played in Fig. 3b. When the parameters are equal to $m_1 = n_1 = 10$, the three first-order rogue waves are separated completely, as shown in Fig. 3c. With the decrease of the parameters α and β, the distance between the second-order rogue waves and the solitons increases by comparing Fig. 3d, e and f. When $\sigma(t)$ is a periodic function and $\gamma_1(t) = 0$, the interactions between the second-order periodic rogue waves and the periodic solitons are presented in Fig. 3g, h and i. If $\sigma(t)$ is changed from $\sigma(t) = \cos(\frac{t}{2})$ to $\sigma(t) = 10\cos(\frac{t}{2})$, it can be observed that the amplitude and shape of the periodic rogue waves and peri-

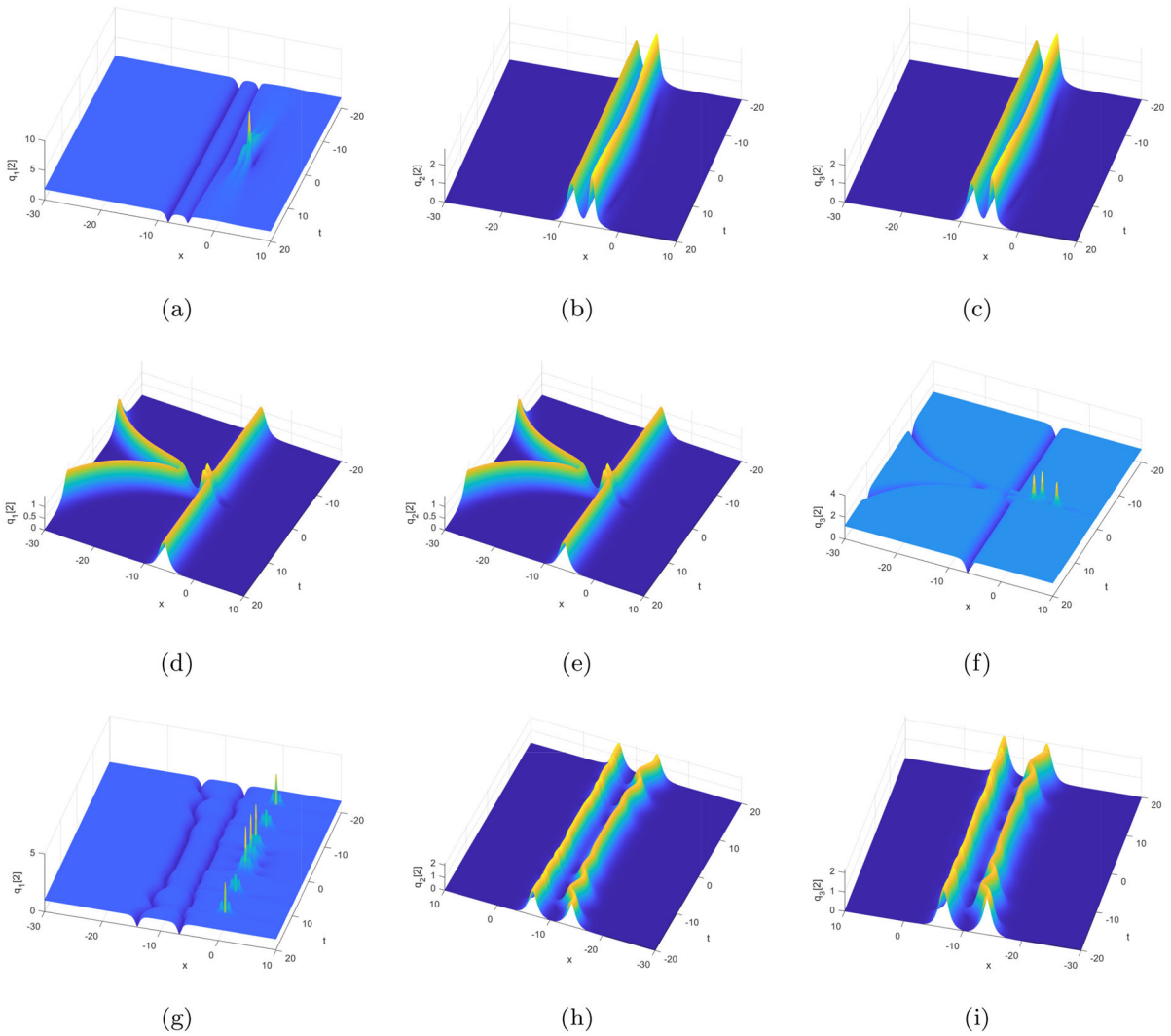

Fig. 4 Evolution diagrams of the second-order localized waves at **a–c** $\gamma_1(t) = 0, \sigma(t) = 0.1, a_1 = 1.8, a_2 = 0, a_3 = 0, \alpha = 0.001, \beta = 0.001, m_1 = 0, n_1 = 0$; **d–f** $\gamma_1(t) = t^2, \sigma(t) = t^2, a_1 = 0, a_2 = 0, a_3 = 1, \alpha = 0.01, \beta = 0.01, m_1 = 10, n_1 = 10$; **g–i** $\gamma_1(t) = 0, \sigma(t) = \cos(\frac{t}{2}), a_1 = 1, a_2 = 0, a_3 = 0, \alpha = 0.001, \beta = 0.001, m_1 = 0, n_1 = 0$.

odic solitons are changed by comparing Fig. 3g and h. Likewise, if the parameters $m_1 = n_1 = 0$ are changed to $m_1 = 100$ and $n_1 = 200$, a row of periodic rogue waves are separated into three rows of ones by comparing Fig. 3h and i.

(4) Figure 4 shows the interactions between the second-order rogue waves and dark-bright solitons. Let $\gamma_1(t)$ and $\sigma(t)$ be constants, Fig. 4a, b and c display the evolution of the second-order rogue waves interacting with two solitons. When $\gamma_1(t) = \sigma(t) = t^2$, the propagation trajectory is of the $''K''$ type for the two solitons, as shown in Fig. 4d, e and f. The second-order rogue waves are separated into three first-order rogue waves and arranged in a triangle under the influence of the separation function $\Omega(\eta)$, as demonstrated in Fig. 4f. When coefficient $\sigma(t)$ is a trigonometric function, the second-order rogue waves are periodic propagation, which can be clearly observed in Fig. 4g, it is difficult to find the periodic rogue waves in the components $q_2[2]$ and $q_3[2]$ in the zero-amplitude background, as exhibited in Fig. 4h and g.

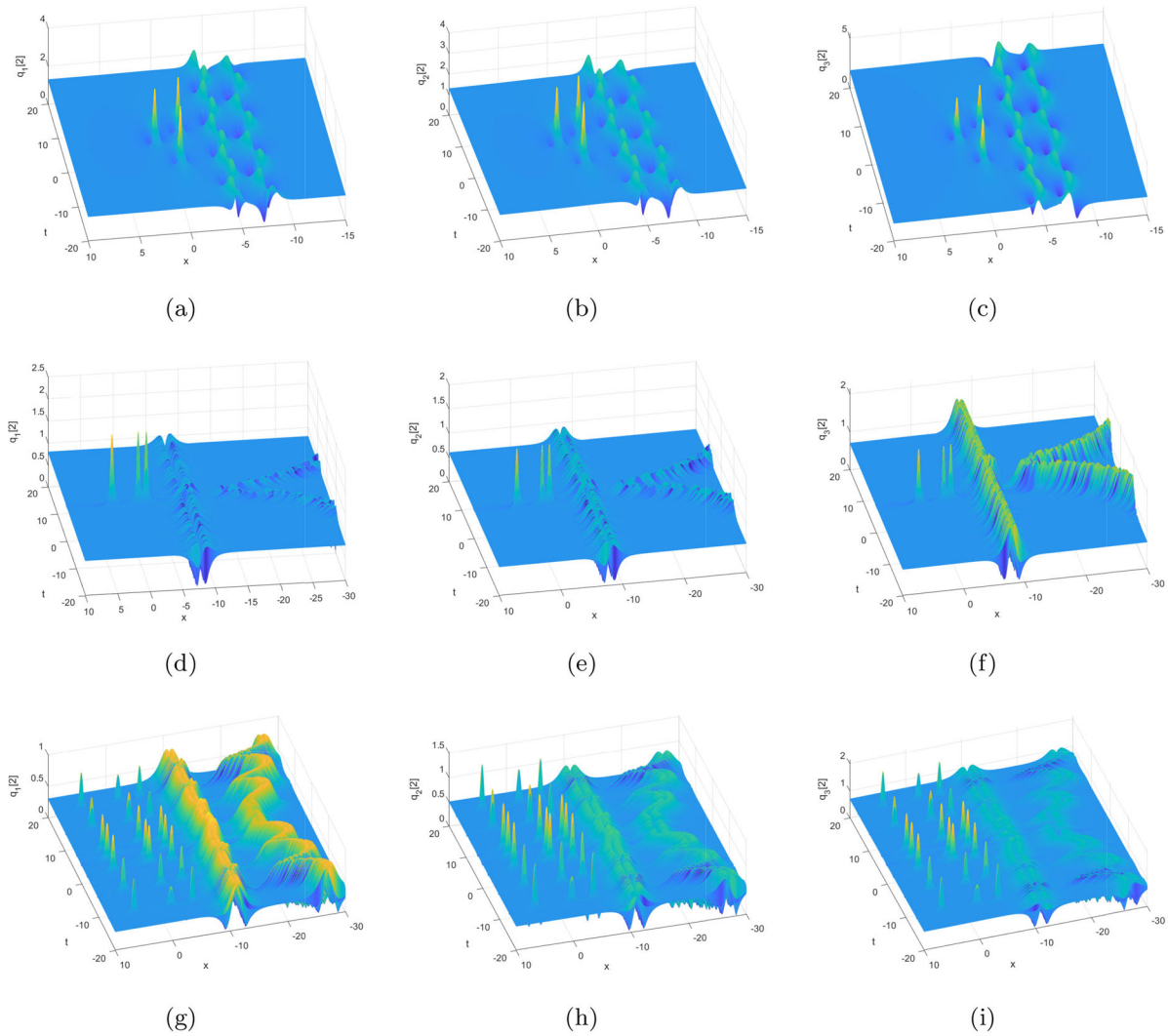

Fig. 5 Evolution diagrams of the second-order localized waves at **a–c** $\gamma_1(t) = 0, \sigma(t) = 0.1, a_1 = 1.3, a_2 = 1.3, a_3 = 1.8, \alpha = 0.0001, \beta = 0.0001, m_1 = 1, n_1 = 1$; **d–f** $\gamma_1(t) = t^2, \sigma(t) = t^2, a_1 = 0, a_2 = 0, a_3 = 1, \alpha = 0.01, \beta = 0.01, m_1 = 20, n_1 = 20$; **g–i** $\gamma_1(t) = 0, \sigma(t) = 10\cos(\frac{t}{2}), a_1 = 0.3, a_2 = 0.5, a_3 = 0.7, \alpha = 0.0001, \beta = 0.0001, m_1 = 50, n_1 = 100$.

(5) Under the condition of $a_i \neq 0\,(i = 1, 2, 3)$, the second-order rogue waves and bright-dark breathers interact with each other in Fig. 5. When the coefficients $\gamma_1\,(t)$ and $\sigma\,(t)$ are constants, the propagation direction of breathers are parallel to the t-axis. The second-order rogue waves consist of three first-order ones, as shown in Fig. 5a, b, and c. When $\gamma_1(t) = \sigma\,(t) = t^2$, the breathers exhibit the shape of $''K''$, and the second-order rogue waves arranged in a triangle, as presented in Fig. 5d, e, and f. If the coeffficient $\sigma\,(t) = 10\cos(\frac{t}{2})$, three rows of periodic rogue waves appear in Fig. 5g, h and i under the influence of the separation function $\Omega\,(\eta)$.

4 Conclusions

Higher-order localized waves for a three-component variable-coefficient fourth-order nonlinear Schrödinger equation are studied by using generalized Darboux transformation. On the basis of the Lax pair and Dar-

boux matrix, the first- and second-order localized wave solutions are obtained. The interactions of solitons, breathers and rogue waves are graphically analyzed. It is demonstrated that the fourth-order dispersion coefficient $\gamma_1(t)$ and the group velocity dispersion coefficient $\sigma(t)$ affect the position and amplitude of the localized waves. When the coefficients $\gamma_1(t)$ and $\sigma(t)$ are constants, the common localized waves occur. When the coefficients $\gamma_1(t)$ and $\sigma(t)$ are exponential functions, the rogue waves interact with the $''V''$-shaped or $''K''$-shaped solitons and breathers. Specially, when the coefficients $\gamma_1(t)$ and $\sigma(t)$ are periodic functions, it is shown that the localized waves generated in the periodic background exhibit the interaction of periodic rogue waves, solitons and breathers. Furthermore, it can be seen that rogue waves are separated under the influence of the separation function. It is hoped that the results will provide some theoretical foundations for the study of optical pulse signal propagation in an inhomogeneous optical fibers, and will be helpful in understanding and predicting the complex behaviors of the localized waves.

Author contributions Ni Song prepared the original manuscript writing and revisions. Yating Liu contributed to the calculation and derivation process, and performed the numerical simulation for the manuscript. Zhuyan Wen analyzed the computational results, and contributed to the interpretation of these results for the manuscript. Wenxiu Ma revised the manuscript for important intellectual content.

Funding This work was supported by National Natural Science Foundation of China (NNSFC) through grant No. 12372026, Natural Science Foundation of Shanxi Province (NSFS) through grant No. 202203021211086 and Research Project Supported by Shanxi Scholarship Council of China (2022-150).

Data availability Data sharing not applicable to this article as no datasets were generated or analysed duringthe current study.

Declarations

Conflict of interest Authors declare that they have no conflict of interests in this work.

References

1. Qi, L., Liu, L., Zhao, W.: Mixed localized waves in the coupled nonlinear Schrödinger equation with higher-order effects. Chaos Solitons Fractals **182**, 114725 (2024)
2. Song, N., Liu, R., Guo, M.M., et al.: Nth order generalized Darboux transformation and solitons, breathers and rogue waves in a variable-coefficient coupled nonlinear Schrödinger equation. Nonlinear Dyn. **111**(20), 19347–19357 (2023)
3. Liu, Y., Wen, X.Y., Wang, D.S.: Novel interaction phenomena of localized waves in the generalized (3+ 1)-dimensional KP equation. Comput. Math. Appl. **78**(1), 1–19 (2019)
4. Wu, X.H., Gao, Y.T., Yu, X., et al.: Vector breathers, rogue and breather-rogue waves for a coupled mixed derivative nonlinear Schrödinger system in an optical fiber. Nonlinear Dyn. **111**(6), 5641–5653 (2023)
5. Veni, S.S., Rajan, M.S.M., Vithya, A.: Controllable Phase shift of optical soliton through nonlinear tunneling in a dual mode optical fiber. Optik **242**, 167094 (2021)
6. Li, L., Cheng, B., Dai, Z.: Novel evolutionary behaviors of N-soliton solutions for the (3+ 1)-dimensional generalized Camassa-Holm-Kadomtsev-Petciashvili equation. Nonlinear Dyn. **112**(3), 2157–2173 (2024)
7. Chabchoub, A., Mozumi, K., Hoffmann, N., et al.: Directional soliton and breather beams. Proc. Natl. Acad. Sci. **116**(20), 9759–9763 (2019)
8. Li, B.Q., Ma, Y.L.: Higher-order breathers and breather interactions for the AB system in fluids. Eur. Phys. J. Plus **138**(5), 1–10 (2023)
9. Yang, B., Yang, J.: Rogue wave patterns associated with Adler-Moser polynomials in the nonlinear Schrödinger equation. Appl. Math. Lett. **148**, 108871 (2024)
10. Djelah, G., Ndzana, F.I.I., Abdoulkary, S., et al.: First and second order rogue waves dynamics in a nonlinear electrical transmission line with the next nearest neighbor couplings. Chaos Solitons Fractals **167**, 113087 (2023)
11. Kumar, S., Mohan, B.: A direct symbolic computation of center-controlled rogue waves to a new Painlevé-integrable (3+ 1)-D generalized nonlinear evolution equation in plasmas. Nonlinear Dyn. **111**(17), 16395–16405 (2023)
12. Chowdury, A., Chang, W., Battiato, M.: Higher-order rogue-wave fission in the presence of self-steepening and Raman self-frequency shift. Phys. Rev. A **107**(5), 053507 (2023)
13. Kumar, S., Mohan, B., Kumar, R.: Lump, soliton, and interaction solutions to a generalized two-mode higher-order nonlinear evolution equation in plasma physics. Nonlinear Dyn. **110**(1), 693–704 (2022)
14. Xu, S.L., Lei, Y.B., Du, J.T., et al.: Three-dimensional quantum droplets in spin-orbit-coupled Bose-Einstein condensates. Chaos Solitons Fractals **164**, 112665 (2022)
15. Lazarides, N., Veldes, G.P., Frantzeskakis, D.J., et al.: Electrostatic wave interaction via asymmetric vector solitons as precursor to rogue wave formation in non-Maxwellian plasmas. Sci. Rep. **14**(1), 2150 (2024)
16. Jadaun, V., Singh, N.R., Singh, S., et al.: Impact of solitons on the progression of initial lesion in aortic dissection. Int. J. Biomath. **15**(03), 2150096 (2022)
17. Ustinov, N.V.: New type of rogue waves. Chaos Solitons Fractals **179**, 114467 (2024)
18. Wang, Y., Huang, L., Yu, J.: N-soliton solutions for the three-component Dirac-Manakov system via Riemann-Hilbert approach. Appl. Math. Lett. **151**, 109005 (2024)
19. Doikou, A., Findlay, I.: Solitons: conservation laws and dressing methods. Int. J. Mod. Phys. A **34**(06n07), 1930003 (2019)
20. Yang, L., Gao, B.: Multiple solitons solutions, lump solutions and rogue wave solutions of the complex cubic Ginzburg-Landau equation with the Hirota bilinear

method. Indian J. Phys. (2024). https://doi.org/10.1007/s12648-024-03242-z
21. Rao, J., Mihalache, D., Zhou, F., et al.: Dark and antidark solitons on continuous and doubly periodic backgrounds in the space-shifted nonlocal nonlinear Schrödinger equation. Chaos Solitons Fractals **182**, 114846 (2024)
22. Raut, S., Barman, R., Sarkar, T.: Integrability, breather, lump and quasi-periodic waves of non-autonomous Kadomtsev-Petviashvili equation based on Bell-polynomial approach. Wave Motion **119**, 103125 (2023)
23. Pu, J.C., Chen, Y.: Data-driven vector localized waves and parameters discovery for Manakov system using deep learning approach. Chaos Solitons Fractals **160**, 112182 (2022)
24. Du, Z., Zhao, X.H.: Vector localized and periodic waves for the matrix Hirota equation with sign-alternating nonlinearity via the binary Darboux transformation. Phys. Fluids **35**(7), 075108 (2023)
25. Lan, Z.Z.: Semirational rogue waves of the three coupled higher-order nonlinear Schrödinger equations. Appl. Math. Lett. **147**, 108845 (2024)
26. Ahmad, S., Saifullah, S., Khan, A., et al.: New local and nonlocal soliton solutions of a nonlocal reverse space-time mKdV equation using improved Hirota bilinear method. Phys. Lett. A **450**, 128393 (2022)
27. Aktosun, T., Unlu, M.: A generalized method for the Darboux transformation. J. Math. Phys. **63**(10), 103501 (2022)
28. Song, N., Guo, M.M., Liu, R., et al.: Localized wave solutions to coupled variable-coefficient fourth-order nonlinear Schrödinger equations. Mod. Phys. Lett. A **39**(09), 2450031 (2024)
29. Du, Z., Tian, B., Qu, Q.X., et al.: Characteristics of higher-order vector rogue waves to a coupled fourth-order nonlinear Schrödinger system in a two-mode optical fiber. Eur. Phys. J. Plus **135**(2), 241 (2020)
30. Li, M., Wang, B., Xu, T., et al.: Quantitative analysis on the bifurcations and exact travelling wave solutions of a generalized fourth-order dispersive nonlinear Schrödinger equation in Heisenberg spin chain. Chaos Solitons Fractals **145**, 110767 (2021)
31. Xu, T.Y., Tian, S.F., Peng, W.Q.: Riemann-Hilbert approach for multisoliton solutions of generalized coupled fourth-order nonlinear Schrödinger equations. Math. Methods Appl. Sci. **43**(2), 865–880 (2020)
32. Borluk, H., Muslu, G.M., Natali, F.: On the orbital stability of solitary waves for the fourth order nonlinear Schrödinger equation. Preprint at arxiv: 2405.09268 (2024)
33. Zhou, X.M., Tian, S.F., Zhang, L.D., et al.: Vector breather waves and higher-order rouge waves to the coupled higher-order nonlinear Schrödinger equations. Int. J. Comput. Math. **98**(12), 2504–2513 (2021)